The development of the Material Plasma Exposure eXperiment MPEX

J. Rapp, T.M. Biewer, T.S. Bigelow, J.B.O. Caughman, R.C. Duckworth, R.J. Ellis, D.R. Giuliano, R.H. Goulding, D.L. Hillis, R.H. Howard, T.L. Lessard, J.D. Lore, A. Lumsdaine, E.J. Martin, W.D. McGinnis, S.J. Meitner, L.W. Owen, H.B. Ray, G.C. Shaw, V.K. Varma and the MPEX team

Fusion and Materials for Nuclear Systems Division
Oak Ridge National Laboratory
Oak Ridge, TN, USA
rappj@ornl.gov

***Abstract*—The availability of future fusion devices such as a Fusion Nuclear Science Facility (FNSF) or DEMO greatly depends on long operating lifetimes of plasma facing components in their divertors. ORNL is designing the Material Plasma Exposure eXperiment (MPEX), a superconducting magnet, steady-state device to address the plasma material interactions of fusion reactors. MPEX will utilize a new high-intensity plasma source concept based on RF technology. This source concept will allow the experiment to cover the entire expected plasma conditions in the divertor of a future fusion reactor. It will be able to study erosion and re-deposition for relevant geometries with relevant electric and magnetic fields in-front of the target. MPEX is being designed to allow for the exposure of a-priori neutron-irradiated samples. The target exchange chamber has been designed to undock from the linear plasma generator such that it can be transferred to diagnostics stations for more detailed surface analysis. MPEX is being developed in a staged approach with successively increased capabilities. After the initial development step of the helicon source and ECH system, the source concept is being tested in the Proto-MPEX device. Proto-MPEX has achieved electron densities of more than $4x10^{19}m^{-3}$ with a large diameter (13cm) helicon antenna at 100 kW power. First heating with microwaves resulted in a higher ionization represented by higher electron densities on axis, when compared to the helicon plasma only without microwave heating.**

Keywords—component; plasma-facing components; Power plants; R&D facilities; plasma-material interactions

I. INTRODUCTION

One of the primary functions of plasma facing components (PFCs) is to exhaust the power leaving the core plasma. Present technologies are capable of exhausting steady-state heat fluxes of up to 10 MW/m^2 [1]. Tungsten based PFCs may be restricted to $5MW/m^2$ in the reactor environment [2], and increasing this level using low-activation materials as required in a neutron environment is an active research area [3]. Novel solutions like liquid metal PFCs, cascading pebble divertors and coated refractory PFCs should be studied as well. In addition to the steady-state heat flux, the transient heat fluxes due to mitigated ELMs will also have to be handled (up to 1 GW/m^2 for 1 ms). Successful development of PFCs that can withstand (steady-state and transient) high heat fluxes is one of the grand challenges for the development of a viable fusion energy source. Important PMI research topics include the melt-layer dynamics of metal PFCs, thermo-mechanical stress analysis of PFCs exposed to many heat flux cycles and ELM transients, and the impact of neutron irradiation on the thermo-mechanical properties. The divertor is also exposed to high ion fluxes ($\Gamma > 10^{24}$ $m^{-2}s^{-1}$) [4] and fluences, which lead to erosion/re-deposition and surface layer modifications. These processes depend strongly on both the material composition, and on the plasma characteristics near the PFC surface. Conditions vary from a 'detached', cold and very dense plasma at the strike point to a hotter 'attached' plasma with reduced density a short distance into the scrape-off layer. The detached (cold and very dense plasma) region is expected to be one of net deposition due to minimal physical sputtering, leading to non-linear surface morphology changes and potential release of dust particles. The attached (hotter but reduced density plasma) region would limit PFC lifetime due to large net erosion. In a reactor (with tungsten PFCs) the net erosion yield has to be lowered to below 10^{-6}, which requires a significant amount of prompt re-deposition of the eroded ions at those electron temperatures. In addition the erosion might be affected by the neutron radiation resulting in enhanced sputtering yields or macroscopic erosion due to whole grain ejection. Control of the tritium inventory is absolutely crucial from points of view of both safety [5] and fuel economy [6]. The diffusion and permeation of hydrogenic species within the bulk material is strongly temperature dependent [5] and thus it is important to investigate retention in the temperature range of future fusion reactors. Furthermore, retention depends strongly on the fluence. However, experimental data are at present limited to a maximum of 10^{27} - 10^{28} D/m^2. Some measured values show an indication of saturation at these high fluences, while other measurements show no saturation in retention. This clearly indicates the need for future experiments substantially beyond the 10^{28} D/m^2 fluence level. Finally, it is expected that hydrogen will also be trapped in

neutron-produced trap sites indicating the need to study the retention properties of irradiated samples. Helium production in the material due to neutron irradiation and implantation of the fusion ash will also change the microstructure of PFCs with synergistic effects on all the above mentioned research issues.

Much of the needed plasma material interaction (PMI) studies and PFC development could be performed in a simplified geometry (i.e., in linear plasma devices), provided that relevant plasma parameters can be reached. The new advanced plasma generator, MPEX, is proposed to address the challenges described above utilizing a new high-intensity plasma source concept. This device will be well suited to test neutron irradiated material samples as well. With these capabilities it will expand the plasma material science significantly over other advanced plasma generators currently coming into operation [7]. It will contribute to the development of a fusion energy source with magnetically or inertially confined plasmas by providing the science of power exhaust under extreme conditions.

II. The Material Plasma Exposure eXperiment (MPEX)

A. Concept of MPEX

Most of the design requirements have already been introduced in [8]. Scoping studies [9] and more detailed plasma fluid/MC neutral modeling [10] has shown that a device length of about 5-6 m is sufficient to reach the required plasma parameters at the target, assuming plasma source parameters which are within reach.

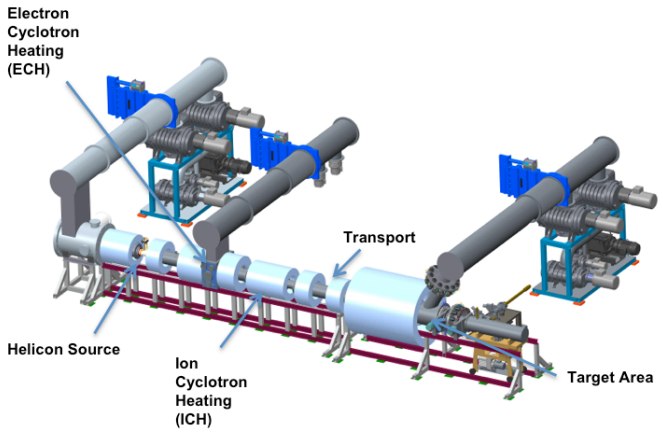

Fig. 1. Conceptual model of MPEX.

The plasma source for MPEX will be based on RF technology [9]. The plasma production will be facilitated by power coupled through a helicon wave antenna at a frequency in the range of 10 - 20 MHz. In MPEX, this helicon produced source plasma will be heated in addition with RF in the electron cyclotron resonance frequency (ECRF) range and in the ion cyclotron resonance frequency (ICRF) range to increase pre-dominantly the electron temperature and total heating power density. Two heating schemes in the electron cyclotron range that allow power coupling to the core plasma despite overdense ($\omega_{pe} > \omega_{ce}$) conditions are being tested: (a) whistler wave electron cyclotron heating (ECH), which propagates in the plasma from high magnetic field side to the resonance magnetic field region and (b) electron Bernstein waves (EBW), which propagate in the plasma from the low magnetic field side to the resonance magnetic field region. In addition the plasma will be heated with ICRH.

Work supported in part by the US DOE under Contract No. DE-AC05-00OR22725 with UT-Battelle, LLC.

B. Advantage of MPEX

In addition to the advantages listed above over toroidal devices, the particular approach of MPEX has also several advantages over other linear plasma wall interaction simulators:

1. The RF source system will minimize the production of intrinsic impurities. This is an advantage over linear plasma devices with internal electrodes in the source system.
2. The heat flux to the target, as well as the plasma parameters in front of the target, will be determined by the conduction limited transport parallel to the magnetic field just like in a SOL of a toroidal device. This will allow investigations of heat flux dissipation and impurity transport similar to the SOL of a toroidal device, which is not possible in other linear devices, where energy transport is often convection driven.
3. A high-power thermal plasma in front of the target allows the investigations of PMI in realistic geometric environments (target at oblique angle to magnetic field) with realistic E and B fields in the sheath. This is different from other linear plasma devices which either have to make use of electrostatic biasing to reach significant heat and particle fluxes on the target, or are influenced by instabilities driven by internal currents between the electrodes.

III. Pre-design of MPEX

A. Helicon plasma source

RF plasma sources in the frequency range 100 kHz to 100 MHz have been used for the production of processing plasmas, ion sources, propulsion systems and other applications. RF power is often coupled in capacitively or inductively in these cases. One effective plasma source is the helicon source (see Fig. 2). The helicon antenna generates standing and propagating waves. It has the advantage that the emitted circular polarized electromagnetic waves are not strongly damped at the plasma edge and can couple power into the core plasma even at higher plasma density. This is of particular interest for our application, since high densities are required.

The MPEX system utilizes a dual half turn helical antenna, shown in Fig. 2. Power is coupled into the plasma through the antenna at a frequency of 13.56 MHz. The antenna is located in air and the power is coupled through an aluminum nitride cylinder (referred to here as a “window”) forming the vacuum boundary in this region.

The antenna is located outside of the vacuum due to the fact that high neutral pressures in the range 0.1 – 3 Pa are

required in the helicon section in order to produce the required plasma densities, and at this pressure and power level antenna sputtering would otherwise be likely to occur that could contaminate material samples being tested.

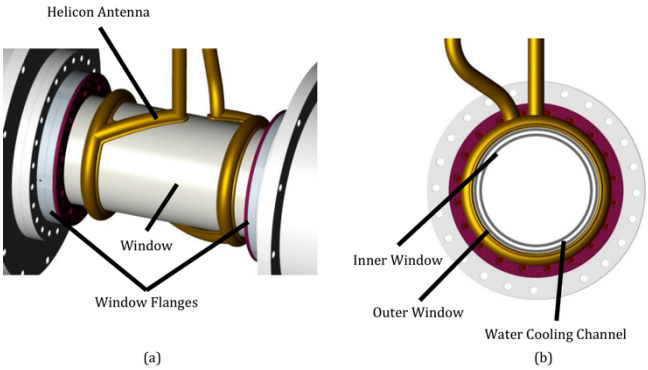

Fig. 2. Helicon plasma source and window.

However, a drawback is that up to 20% of the power launched by the antenna is deposited on the inner surface of the window due to rf-plasma sheath interactions and the production of hot neutrals. The window thus must be adequately cooled so that thermal stresses do not become excessive. In order to reduce stresses, aluminum nitride (AlN) is being used for the window material in the present test program due to its very high thermal conductivity.

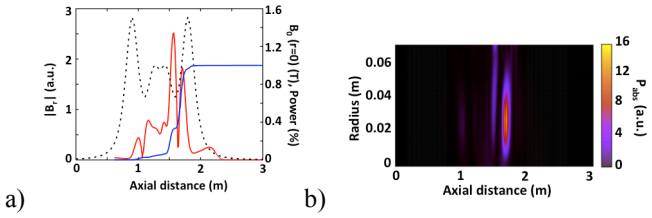

Fig. 3. Example of EMS2D calculation with axially non-uniform background magnetic field: a) Helicon wave confinement and axial power deposition profile in a magnetic mirror. RF magnetic field amplitude (red), background magnetic field (dashed), integrated fraction of absorbed power (blue); b) 2-D view of absorbed power density showing good radial penetration to the axis.

The antenna helices have a left handed twist in order to couple to the predominantly right hand circularly polarized fast wave, or 'helicon' wave, that propagates in the frequency range between the ion and electron cyclotron frequencies [11]. At the magnetic field strengths of interest ($\geq$ 0.1 T near the antenna and higher elsewhere), the operating frequency is less than the lower hybrid frequency. The slow wave does not couple in this frequency range, and power coupling is through the fast wave. It is believed that power is transferred from the wave to the electrons primarily through collisional damping, enhanced by the presence of eigenmodes and focusing due to the non-uniform axial magnetic field profile [12-14]. The antenna is located in a region with a nearly uniform axial magnetic field profile, but there is a magnetic peak located towards the target. This has been found to be necessary to achieve high plasma densities in hydrogen or deuterium plasmas [13]. For the MPEX magnetic field configuration, modeling using the EMS2D code has demonstrated that the helicon waves are reflected by the downstream (as well as upstream) magnetic field peaks with radial boundary conditions also playing a role [15]. This also increases total damping. Figs. 3a and b show an example of EMS2D calculations, indicating confinement of the wave electric field in the magnetic field gradient.

As MPEX will be a steady-state device, the helicon antenna, and in particular its window, have to be water-cooled. It is the plan to add a water channel to the window by adding a larger diameter secondary cylindrical window located coaxially with the first with a narrow gap in between the two. As the thickness of the window increases, the distance between the antenna and plasma does as well and the plasma coupling drops. The windows procured for the experiments to-date have a 6 mm wall thickness. Manufacturing windows of the required length and diameter with thinner walls will be difficult, but, may be possible with a development effort involving suppliers. For the purpose of this study, we have examined the electrical performance of two water cooled windows: one with 3 mm thick inner and outer window, and the second with a 6 mm thick inner window and 3 mm thick outer window. These have been compared to the existing single 6 mm thick window. The high thermal conductivity is not needed for the outer window since the only heat deposited in it arises directly from the RF and is greatly reduced in comparison to the inner window. This window can be made from a more common material such as alumina and can likely be made with a thinner wall. The antenna itself also has a design feature that maximizes coupling. It is comprised of flat straps (Fig. 2) so that RF currents in the helices can travel as close to the plasma as possible. Semicircular channels welded to the straps on the outside carry the water used to cool it. It would be simpler to fabricate an antenna directly out of circular tubing, but in this case the current on the average would be located at a larger radius reducing the plasma coupling.

The 3-D electromagnetic modeling code CST Microwave Studio (MWS) has been used to examine the three cases described above. For the water-cooled designs there is assumed to be a 1 mm thick water channel between the inner and outer windows. The code has been used to determine the relative loading for these cases, and utilizing that quantity, the input current required to couple 100 kW of RF power to the plasma. The current has then been used in turn to scale the electric fields calculated by MWS for the different configurations. The electric field is the factor that limits the peak power while power deposition and cooling considerations determine long pulse power limits. Figure 4 shows the MWS model for the case with the 6 mm thick inner window and 3 mm thick outer window. The water channel can be clearly seen as well as the gap between the outer ceramic and the antenna, which for all cases is taken to be 4 mm. In order to minimize the mesh size, the model assumes as a boundary condition that all regions not containing vacuum (transparent blue region), plasma, or components are filled with perfect electrical conductor (PEC). The antenna is also

modeled as PEC. In this model, a lossy dielectric is used to model the plasma. The dielectric constant for the two windows is assumed to be the same (=9.5) and the water in the cooling channel is modeled using the dielectric constant and conductivity of pure water.

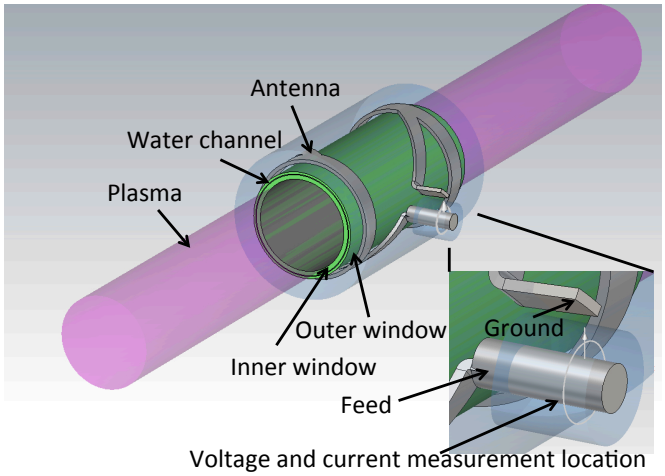

Fig. 4. MWS model of helicon antenna with double window.

The input power is determined by using the usual formula $P_{in} = ½ \mathrm{Re}(VI^*)$, where V and I are the complex input voltage and current respectively, and the asterisk denotes that the complex conjugate should be taken. The antenna resistive coupling is then simply $R_a = 2P_{in}/I^2$. The voltage is measured between the inner and outer conductor of the feed at the location indicated by the arrow in the model, and the current is obtained by integrating the tangential RF magnetic field around the circle at the same location. The results are given in Table I. Looking at the plasma coupling R_a first, virtually identical for the case with the single 6 mm thick window, and that with two 3 mm thick windows and a 1 mm gap in between. If the thickness of the inner window is increased by 3 mm, then the coupling drops by ~30%.

TABLE I. ELECTRICAL PERFORMANCE FOR THREE HELICION WINDOW CONFIGURATIONS

Configuration	P_{in}	R_a	$\lvert E_{max}\rvert$
6 mm	0.07 W	2.23 Ω	1.3 kV/mm
3 mm + 1mm gap + 3 mm	0.058 W	2.26 Ω	1.3 kV/mm
6 mm + 1 mm gap + 3 mm	0.048 W	1.50 Ω	1.8 kV/mm

It is important to note that only the relative values are important here. Because MWS does not include a plasma model using an isotropic lossy dielectric instead, the absolute value of the loading is not expected to be modeled accurately. In actual experiments with the existing 6 mm thick window, the resistive plasma coupling has been measured to be ~ 6 Ω for both deuterium and helium plasmas, even at relatively low density of 1 - 2 x 10^{19} m^{-3} (fig. 5). The scaled loading based on the experimentally measured value is then 6 Ω for the second case and 4 Ω for the third. P_{in} from the Table 1 is then used to scale the current from the model, which is not shown in the table, but is ~ ¼ A. The scaled peak input current for 100 kW power, also taking into account the scaled loading is then 183 A for the first two cases and 224 A for the third. The maximum electric fields from MWS, using the scaled currents are also given in Table I.

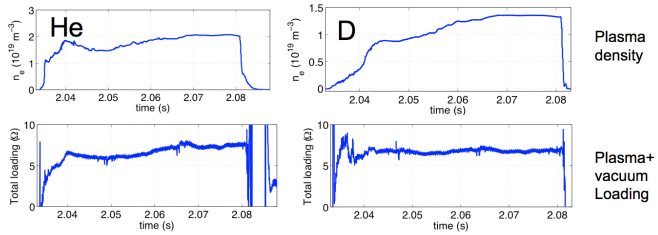

Fig. 5. MWS model of helicon antenna with double window.

Figures 6 and 7 show the MWS modeling of the electric field magnitude in the vicinity of the antenna feed, where the field is maximum, for the case with a 6mm thick inner window and 3 mm thick outer window. As would be expected, the field peaks in the gap between the antenna and the outer ceramic. For the worst case, the maximum electric field of 1.8 kV/mm is still well below the limit in ambient air of ~ 2.7 kV/mm, which suggests it may be possible to increase the outer window thickness if necessary.

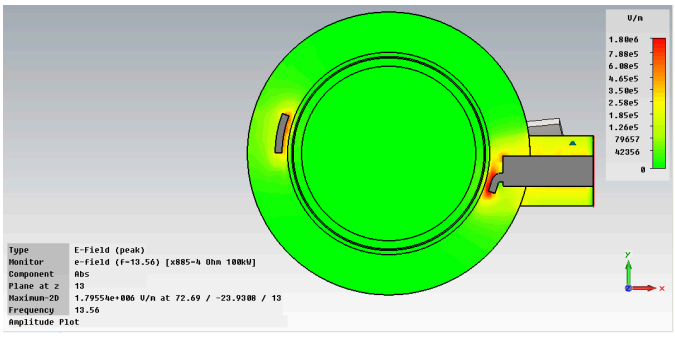

Fig. 6. MWS simulation of RF electric field magnitude at the axial location of the field maximum.

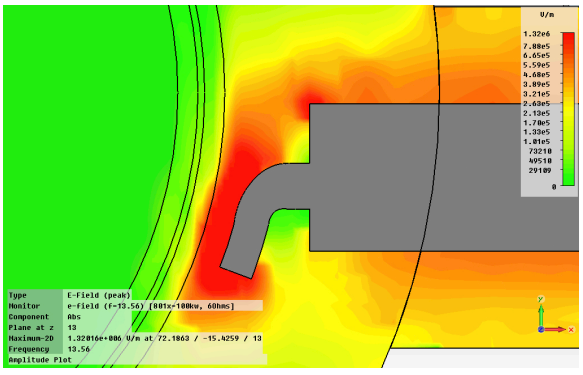

Fig. 7. Close-up showing electric field magnitude peaking in the gap between the antenna feed and the outer window.

B. ECH heating system

Electron heating of the plasma is essential to get into the conduction limited plasma transport regime, the underlying principle of the device. Electron Bernstein Wave heating is planned to be the heating scheme of choice, since the ordinary electromagnetic waves in the electron cyclotron range will not propagate in the envisioned density range and magnetic field range planned in MPEX. Electrostatic electron Bernstein waves (EBW) propagate in those over-dense plasmas in which the plasma frequency is larger than the electron cyclotron frequency. In the scenario for MPEX, a double mode conversion from an obliquely launched O-mode via the slow branch of the X-mode to the EBW is planned, meaning EM waves in the electron cyclotron frequency domain are launched into a magnetic mirror from the low field side to the electron cyclotron resonance layer in the magnetic mirror (1.6 T). An existing 28 GHz gyrotron is used supplying 200 kW steady-state power. The 28 GHz gyrotron with its power supplies is already installed as part of the phase-II development phase to MPEX (Proto-MPEX). It is planned to include a splitter in the waveguide to Proto-MPEX and route a waveguide branch to MPEX.

The main modifications to the ECH systems are related to the steady-state demands of MPEX. For MPEX, adding water cooling to mirrors used with the Proto-MPEX design is planned. There are two in-vessel copper mirrors fed by an open end corrugated waveguide. The first mirror will be flat and the second ellipsoidal to provide some beam focusing and to tilt the beam toward the center of the plasma or at a slight angle depending on what is optimum for O-X-EBW mode conversion. A waveguide vacuum window will be just outside the vacuum vessel.

For the window, an existing double-disk FC-75 cooled window rated to 200 kW cw will be installed. This window uses FC-75 cooling and is rated to 200 kW cw. Later, if it proves necessary to increase reliability and improve safety, a lower cost CVD diamond disk will be acquired to replace the face-cooled double disk unit with a single disk edge water cooled unit thereby eliminating the FC-75 pumping system, heat exchanger and potential to damage turbo pumps if the vacuum side disk were to break due to metallization from plasma sputtering.

C. ICH heating system

Direct ion heating will be used to increase ion energies to 30 eV or more. This will be accomplished using ion cyclotron heating (ICH), specifically single pass damping of a slow wave launched from the high field side into a magnetic beach. Slow wave beach heating has long been recognized as an efficient means to couple power into a single species plasma, as demonstrated in the 1960's on the B66 device [16], and later on tandem mirrors including Phaedrus [17], Tara [18], and others. Efficient single pass damping of slow waves has been previously observed on Phaedrus in the context of ion trapping [19] and more recently on the VASIMR VX-50, which is similar to MPEX in that the ICH is used to heat a high density target plasma produced by a helicon plasma generator. In this experiment, ICH power coupling efficiency $\geqslant$ 80 % and ion energies up to 200 eV were achieved for deuterium plasmas [20].

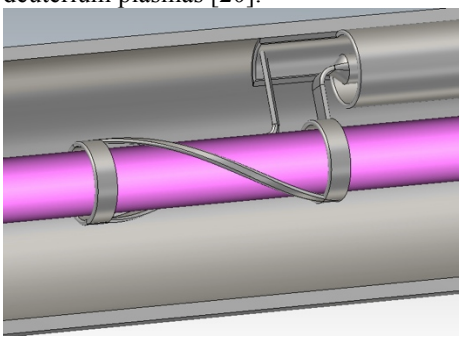

Fig. 8. View of ICH antenna concept including coaxial feedline.

In MPEX, the power will be coupled through one or two modified Nagoya Type III antennas with half-turn helical twists, similar to the helicon antenna, but with the opposite helicity (see Fig. 8). This is the type of ICH antenna used in the VASIMR experiments. It efficiently couples to the n=-1 azimuthal slow wave mode in the plasma, which is predominantly left-hand circularly polarized. Because the neutral pressure in the ion cyclotron heating region is necessarily much lower than that in the helicon region, in order to prevent excessive charge exchange losses, the antenna can be mounted in the vacuum chamber without producing significant sputtering. This also requires the use of limiters nearby that greatly reduce the connection lengths of field lines mapping to the antennas and thus minimizes the plasma density in their vicinity. The use of an internal antenna allows the plasma loading to be maximized, which is important in order to allow the design value of 200 kW input power per antenna to be achieved. Because of the internal location, and the fact that |B| is higher at the location of the ICH antenna than at the helicon antenna, the diameter of the former is less than the latter and will be in the range of 8 – 12 cm.

D. Magnet system

The magnet system for MPEX consists of five systems (Helicon, ECH, ICH, Transport, & Target) that can be operated independently, but, work together with the vacuum and rf systems to produce a plasma density at the target area that is beneficial for accelerated testing of plasma materials for fusion environments. This pre-conceptual design study examined the coil configuration for each system that would perform within the dimensional constraints that were provided by the other systems and allow for continuous operation. Fig. 9 shows the layout and relative size of the magnet system relative to the different components of MPEX.

The design of the magnet system focused on conductor material that could best provide fields on the order of 2.0 T for plasma generation and heating and 1.0 T within the target area. Given the desire to operate the system in a continuous mode in each section of MPEX, low temperature superconducting (LTS) magnets were selected. This selection was driven by the maturity of the conductor technology as

well as other supporting technologies relative to alternatives currently commercially available.

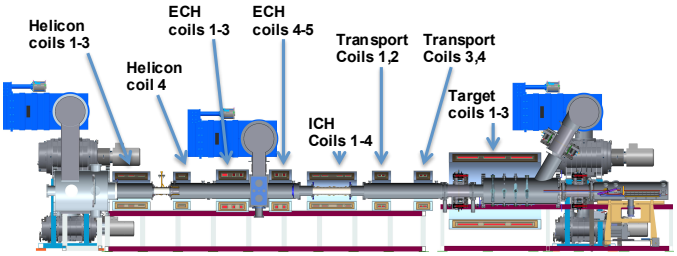

Fig. 9. Layout and relative size of the magnet system.

With respect to the magnet composition and design philosophy, the magnets for MPEX were designed starting with the properties of commercially available NbTi conductor. Once the optimum field profile was set with feedback from each system that the magnets support, the coil winding geometry was optimized to keep the current in each coil between 100 A and 200 A in order to minimize the heat leak from the current leads and assure that the forces of the magnets were within engineering limits of existing available structural materials. In total, there are twenty separate LTS solenoids that compose MPEX.

For the cryogenic cooling of the MPEX superconducting magnets, separate liquid helium condensing cryo-cooler systems were chosen over a closed cycle liquid helium refrigeration system. This was chosen for several reasons. Given the nature of the MPEX assembly and potential maintenance and access required for the different supporting systems, the ability to remove each magnet system in a modular fashion is an advantage from an access point-of-view as well as reducing the potential contamination of the cooling system that would result from disconnecting transfer lines and other ancillary equipment that are attached to the magnets. In addition, separate cryo-coolers as re-condensers that operate in a fairly static manner, reduce the number of moving parts for the circulation pumps and valving that increase reliability and availability of the system. Another benefit to the cryo-cooler-based system is the lack of complexity that comes with a closed cycle liquid helium refrigeration system with intricate filtering, heat exchangers, and processing of the return flow from the superconducting coils that adds additional control monitoring and maintenance.

While the efficiency of a closed cycle, liquid helium refrigeration, typically a reverse Brayton system, is higher than the pulse tube cryo-cooler re-condensing system, this advantage is not significant enough to overcome the benefits mentioned previously.

The cryogenic envelope for the the MPEX magnets is shown schematically in Fig. 10. Essentially, the first stage of the cryo-cooler is anchored to the “40 K thermal shield” to intercept the heat loads that are associated with the room temperature connections between the cryostats and the magnet. This is driven primarily by the mechanical support structure as well as the current lead feedthroughs.

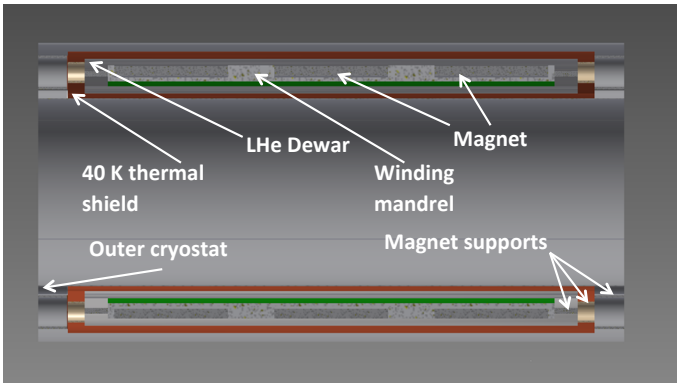

Fig. 10. Cryogenic envelope for calculations of heat loads for cryocooled helium recondensing systems as part of MPEX magnets.

The second stage of the cryo-cooler serves to maintain the liquid helium at a volume of 30 to 500 liters depending on the size of the magnets. This design is based on commercially available systems that have been successfully fabricated in the size and magnetic field range of the majority of the MPEX magnets.

TABLE II. ESTIMATED REFRIGERATION HEAT LOADS, REQUIRED NUMBER OF CRYOCOOLERS, AND LHE RESERVOIR FOR EACH MPEX CRYOSTAT

No	*Coil description*	*Total heat load 1st*	*Total heat load 2nd*	*No of cryo-coolers*	*Size of LHe reservoir*
1	Helicon coils 1 - 3	39W	1.7W	2	80 l
2	Helicon coil 4	15 W	0.4W		40 l
3	ECH coils 1 - 3	31W	1.2W	2	210 l
3	ECH coils 4, 5	20W	0.6W	2	70 l
4	ICH coils 1 – 4	38W	1.0W	2	112 l
5	Transport coils 1, 2	31W	1.2W	2	33 l
6	Transport coils 3, 4	30W	1.0W	2	33 l
7	Target coils 1 - 3	72W	5.5W	6	500 l

Table II breaks down the estimated total heat load of each stage of the cryo-coolers as well as the number of cryo-coolers for each cryostat. The number of cryostats was selected to minimize the number of room temperature to cryogenic penetrations for structural support of the magnet. With a commercially available water-cooled cryo-cooler system, the refrigeration power for the first and second stage of the cryo-coolers was assumed to be 40 W at 40 K and 1.5 W at 4.2 K respectively. To provide some margin, an additional cryo-cooler was added to each cryostat except for the target cryostat where two were added. It should be stated that the cryo-cooler will be used primarily for the operational and limited number of shutdown scenarios where the outages are on the order of hours.

A passive quench protection system should be sufficient to protect each coil with the majority of the energy dissipated in the magnet. Given the size of the target coils additional effort is likely needed during the conceptual design stage of the MPEX design to determine whether further subdivision of the coils would be advantageous for quench protection.

E. Vacuum system

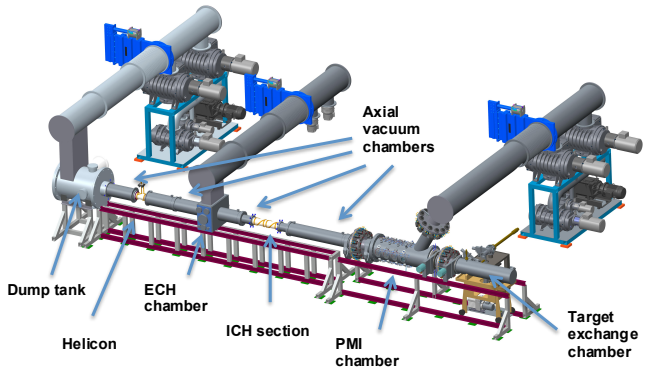

Fig. 11. Overview of the vacuum system.

The vacuum chamber consists of a PMI chamber, a dump tank on the opposite side, and cylindrical tubes connecting the plasma source with the RF heating regions to the PMI chamber and dump tank (see Fig. 11). All vacuum chambers are water cooled and are made of stainless steel except for the helicon antenna window as described above. The heat deposition on the helicon antenna window is too large to cool the window from the edges, so the surface must be water-cooled. The water-cooling channel will be created by concentrically nesting two AlN tubes or possibly an inner AlN tube with an outer alumina tube. The window will be soldered to stainless steel knife edge flanges with annealed copper gaskets at each end, which are bolted into the main vacuum chamber. The flanges will provide fitting for the water cooling inlet and exhaust. The plasma is tightly constrained radially in the helicon window 138 mm diameter.

TABLE III. MPEX VACUUM PARAMETERS

	Pressure [Pa]
Upstream dump tank	1-10
PMI chamber	1-10
Helicon antenna	0.1-3
ECH launcher chamber	0.01
ICH antenna section	0.01
Target exchange chamber after decoupling	10^{-4}
Gas load, steady-state, H_2, D_2	7 slm

Differential pumping has to be employed to fulfill the pressure requirements in the individual heating chambers and target chambers (see Table III).

It is foreseen to utilize large roots blower trains at the PMI chamber and the dump tank, both with a pumping speed of about 22,500 m^3/hr. This will keep the pressure below 10 Pa even at the highest gas flow rate (7 slm). The pumping ducts were dimensioned to 24 inches diameter to each pump train. The ECH chamber, which requires lower pressure, will be pumped by two parallel turbo pumps with a pumping velocity of 2300 l/s each with pump duct diameters of 14 inches.

The PMI chamber is designed such that it can be de-coupled from the plasma generator by an autonomous decoupling system. The PMI chamber can then be moved out of the magnet system axially on a rail system for maintenance purposes.

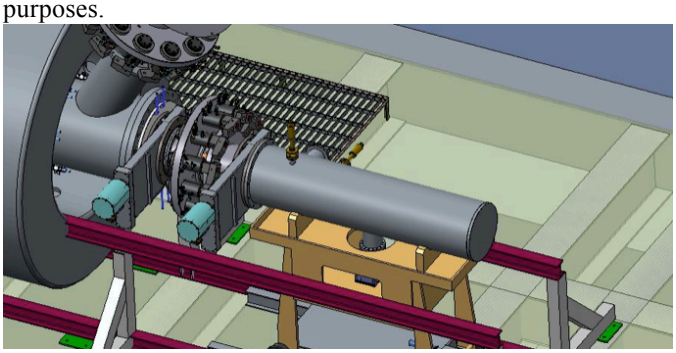

Fig. 12. Target exchange chamber docked to PMI chamber.

Connected to the PMI chamber is the target exchange chamber (Fig. 12), which can be decoupled by the same mechanism as described above to transfer targets for surface diagnostic purposes in-between plasma pulses or for exchange of targets.

IV. DEVELOPMENT PATH OF MPEX

The prototype of the source system is under development in a staged approach. First the helicon plasma production as well as whistler wave and EBW coupling were tested individually by themselves. Table IV shows how the heating power is increased from one test stand to another. Experimental results are shown in the section below. The device Proto-MPEX is used to develop the plasma source concept and to verify the conduction limited transport regime in this linear device.

TABLE IV. MPEX HEATING POWER DEVELOPMENT

	Phase I (2 s) PhIX	***Phase II (2 s) Proto-MPEX***	***MPEX Steady-state***
Helicon	100 kW 13.56 MHz	100 kW 13.56 MHz	100-200 kW 13.56 or 27 MHz
ECH (EBW)	20 kW 18 GHz	200 kW 28 GHz	200 kW 28 GHz
ICH	-	30-200 kW 9-12 MHz	200-400 kW 9-12 MHz
Total	120 kW	330-500 kW	500-800 kW

In addition the effect of the recycling at the target on the plasma source parameters achievable will be studied. Extensive transport simulations with B2-Eirene indicate that with the heating power available, target heat fluxes of 10MW/m^2 should be achievable in MPEX [10] and also for the 500 kW in Proto-MPEX.

A. Pre-Phase I experiments

Before the phase I development stage, stand-alone helicon antenna tests in a mirror arrangment have been carried out. A pre-prototype helicon antenna has been tested at moderate magnetic fields in the antenna region (up to 0.12 T (D), 0.5 T (He)) with coupled heating powers of up to 100 kW. A maximum electron density of $n_e \sim 6.0 \times 10^{19}$ m^{-3} has been achieved in helium discharges at a magnetic field of 0.3 T (see Fig. 13). In deuterium discharges with a magnetic field of ~ 0.12 T electron densities of $n_e > 4.0 \times 10^{19}$ m^{-3} have been achieved.

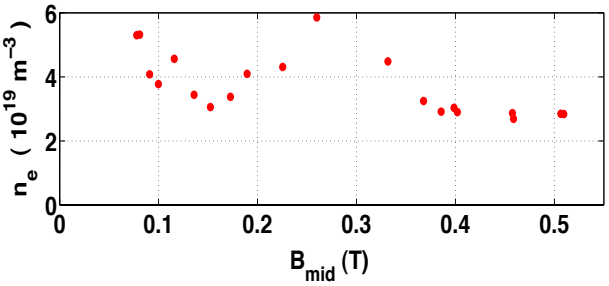

Fig. 13. Electron density in helicon antenna region vs B on axis at helicon antenna midplane, for He discharge.

Electron heating has been investigated in a separate experiment. A target plasma was produced by microwaves (18 GHz) at high magnetic fields of B = 0.9 T, and the electrons subsequently heated. Two concepts have been tested: a high-field launch whistler wave coupler and an Electron Bernstein Wave (EBW) launcher. Electron temperatures in excess of 10 eV have been measured in the device. Furthermore over-dense plasma coupling at 6 GHz has been demonstrated. Evidence of coupling the whistler wave as well as the EBW to a high density plasma was obtained with the addition of either EBW or whistler waves producing a radial peak in the plasma density approximately double the cutoff density at 6 GHz.

B. Phase I experiments (PhIX)

In the phase I experiment, electron densities of about $n_e \sim 2.0 \times 10^{19}$ m^{-3} have been achieved outside of the mirror at minimum magnetic field 1 m away from the helicon section (see Fig. 14) with helium plasmas.

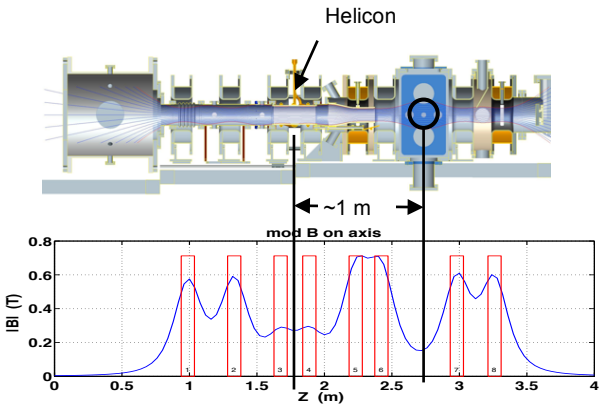

Fig. 14. Cross section of the Physics Integration eXperiment (PhIX) and the axial magneitc profile with indications of the measurement position.

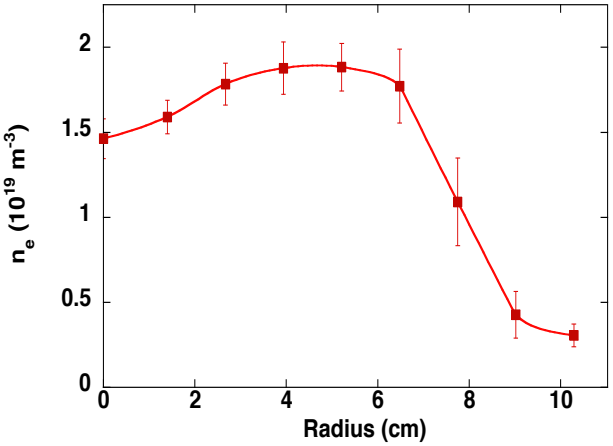

Fig. 15. Radial plasma density profile in a Helium discharge.

At this magnetic field and power level, the plasma has a diameter of about 9 cm with a centrally peaked density profile (Fig. 15). Approximately $n_e \sim 3.0 \times 10^{19}$ m^{-3} has been produced in the helicon region with deuterium. Fig. 16 shows a power scan for deuterium plasmas. In addition to the helicon 7.5 kW of 18 GHz microwave power was injected in those plasmas.

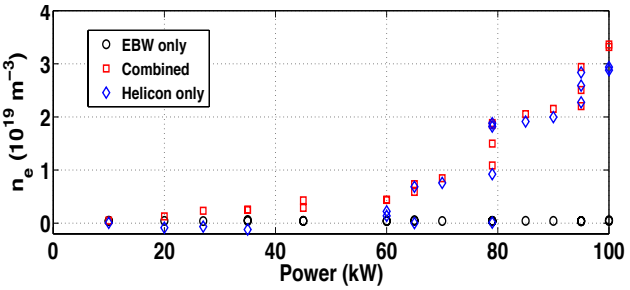

Fig. 16. Electron density for deuterium plasmas on axis in helicon region vs power.

C. *Phase II experiments (Proto-MPEX)*

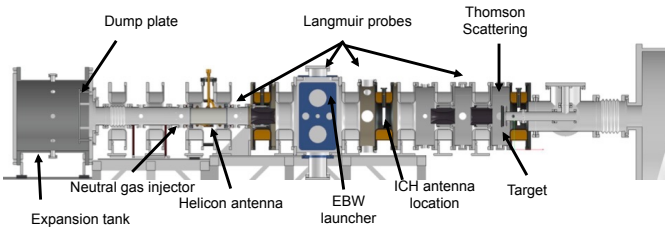

Fig. 17. Cross section of the Proto-MPEX device.

Fig. 17 shows Proto-MPEX. Proto-MPEX will be used to test the combined electron and ion heating of the helicon produced plasma. In total 330 kW are available.

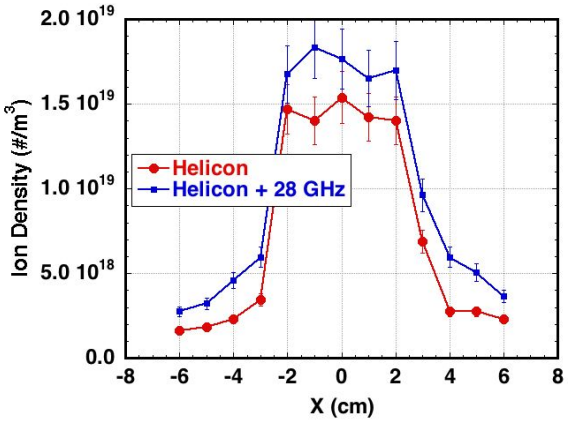

Fig. 18. Ion density with helicon only and with combined helicon and 28 GHz EBW heating. The cutoff density is at 1 x 10^{19} m^{-3}. The ion density is derived from measurements by a Langmuir probe.

First experiments began with launching 28 GHz microwaves into the helicon target plasma. Preliminary measurements (Fig. 18) indicate a significant increase in the core plasma density with the addition of EBW power, even though the density in the region is significantly above cutoff (50% above). The addition of 100 kW EBW to 100 kW helicon plasma producing these results appears cumulative without degradation of the helicon performance noted.

V. Summary and Conclusions

A pre-design of a new advanced linear plasma generator for testing materials and plasma facing components for future fusion reactors has been prepared. The new plasma source concept based on RF heating technology is being developed through dedicated test stands. Experiments demonstrated the production of plasma densities necessary for achieving fusion reactor conditions at the target as predicted by plasma fluid/MC neutral modeling. First electron heating experiments with 100 kW EBW with 100 kW helicon produced plasmas have been performed demonstrating coupling to over-dense plasmas.

References

[1] R.A. Pitts et al., *J. Nucl. Mater*. 415 (2011) S957

[2] M. Rieth, EFDA Technical Meeting on DEMO (Garching, Germany September 29-30, 2009)

[3] M. Rieth et al., *J. Nucl. Mater*. 417 (2013) 463

[4] R. Behrisch et al., *J. Nucl. Mater*. 313-316 (2003) 388-392

[5] J. Roth et al., *J. Nucl. Mater*. 390-391 (2009) 1-9

[6] J. Roth et al., *Nucl. Fusion* **44** (2004) L21

[7] J. Rapp et al., Fus. Eng. Des. 85 (2010) 1455-1459

[8] J. Rapp et al., Fus. Sci. Technol. 64 (2013) 237-244

[9] J. Rapp et al., Proceedings of the 24th IAEA Fusion Energy Conference, (8-13 October 2012, San Diego, CA, USA), FTP/P1-33

[10] J. Rapp et al., J. Nucl. Mater. 463 (2015) 510-514

[11] F.F. Chen et al., Phys. Plasmas 3 (1996) 1783

[12] M.D. Carter et al., Phys. Plasmas 9 (2002) 5097

[13] Y. Mori et al., Plasma Sources Sci. Technol. 13 (2004) 424

[14] Y. Mori et al. Thin Solid Films 506-507 (2006) 583

[15] R.H. Goulding et al., AIP Conf. Proc. 1187 (2009) 667

[16] W.M. Hooke et al., Phys. Fluids 8 1146 (1965)

[17] D.R. Roberts and N. Hershkowitz, Phys. Fluids B 4 1475 (1992)

[18] S.N. Golovato et al., Phys. Fluids 31 3744 (1988)

[19] S.N. Golovato et al., Phys. Fluids 28 734 (1985)

[20] E.A. Bering, et al., Phys. Plasmas 17 043509 (2010)